Flux-Map Based FEA Evaluation of Synchronous Machine Efficiency Maps

The elastic modulus variation during the shotcrete curing jointly investigated by the convergence-confinement and the hyperstatic reaction methods

Pierpaolo Oreste[1], Giovanni Spagnoli[2], Cesar Alejandro Luna Ramos[3]

[1] Department of Environmental, Land and Infrastructural Engineering, Politecnico di Torino, Corso Duca Degli Abruzzi 24, 10129 Torino, Italy, ORCID: 0000-0001-8227-9807

[2] BASF Construction Solutions GmbH, Dr.-Albert-Frank-Straße 32, 83308 Trostberg, Germany, Phone: +49 8621 86-3702, *http://orcid.org/0000-0002-1866-4345*, E-mail: *giovanni.spagnoli@basf.com* (corresponding author)

[3] Faculty of Engineering, Universidad Mariana, Calle 18 No. 34-104 Pasto, Colombia, celuna@umariana.edu.co

ABSTRACT

Induced stresses in sprayed concrete (or shotcrete) are quite complex to evaluate and depend on many factors such as the size and depth of the tunnel, the geomechanical characteristics of the surrounding ground in which the tunnel is excavated, the type of shotcrete, the evolution of its mechanical parameters over time and the excavation face advance rate. In particular, the evolution of the mechanical properties of the shotcrete is crucial regarding the interaction with the tunnel wall and the development of the bending moments and the normal forces which occur along the circumference of the lining. In this research, a new calculation procedure based on the combined use of two calculation methods the Convergence Confinement Method (CCM) and the Hyperstatic Reaction Methods (HRM) is presented. Thanks to this procedure, it is possible to progressively apply the load acting on the lining as the curing phase of the concrete progresses and therefore with the evolution of its mechanical parameters. This procedure has been applied to several examples of calculation, obtaining useful considerations regarding the mechanical behavior of the shotcrete lining when some fundamental parameters of the calculation change. As it is possible to achieve bending moments and forces in the lining with the progress of the load steps. It is also possible to determine the trend of the lining safety factor over time and at the end

of the loading phase, allowing a proper design of the support, with particular attention to the type of shotcrete and the thickness of the lining.

Keyword: Hyperstatic reaction method; Convergence confinement method; lining; shotcrete; rock; curing

NOTATION LIST

A	Area of the lining section
E_{rm}	Elastic modulus of the rock mass
$E_{,mean}$	Mean value of the elastic modulus of shotcrete
$E_{,t}$	Elastic modulus of shotcrete at the time t
$E_{,0}$	Value of the asymptotic elastic modulus of the shotcrete, for $t = \infty$
$\{F\}$	Nodal forces applied to the numerical model
J_z	Moment of inertia of the lining section
K	Global stiffness matrix
k_i	Local stiffness matrix of the element i;
K_n	Normal stiffness of the interaction spring in the node of the model
K_0	Lateral earth pressure
K_s	Shear stiffness of the interaction spring in the node of the model
l	Length of the one-dimensional element
M	Bending moment
N	Normal force
p	Internal tunnel pressure
p_{cr}	Critical pressure at the limit between the elastic and the plastic behavior
p_{fict}	Fictitious internal tunnel pressure
p_0	Lithostatic pressure
R	Tunnel radius
r	Generic radial coordinate
$\{S\}$	Vector of nodal displacements
T	Shear force
t_0	Final installation time of the support
u	Tunnel wall radial displacement
v	Poisson's ratio
α	Time constants (t^{-1}) of the curing equation for the elastic modulus
α_i	Angle of inclination of the element ith with respect to the horizontal
ϕ	Rotation of the element in correspondence to the nodes

61 δ Advance step

δn nodal normal displacement between the structure and the rock mass

δs shear displacement between the structure and the rock mass

62 $\sigma_{c,t}$ Unconfined compressive strength for the shotcrete at the time t.

63

INTRODUCTION

Sprayed concrete or shotcrete (SC) is pumped under pressure through a pneumatic hose and projected into place at high velocity (30 to 50 m/s), which is compacted and finally cures (DIN 18551, 1992; Thomas, 2009; Hemphill, 2013), see Fig. 1.

Because SC compared with ordinary concrete has a shorter setting time and high early age mechanical properties (Wang et al., 2015), it is normally used for solving stability problems in tunnels and other underground constructions such as mines, hydropower projects and slope stabilization (e.g. Melby, 1994). SC can be employed for temporary and permanent supports. However, regarding the design and construction of modern tunnels, SC single layer lining is becoming the trend of future development (Franzen et al., 2001). With SC as permanent final lining, long-term performance requirements, such as good bonding, high final density, compressive strength and chemical resistance, have to improve (Melby, 1994).

SC mechanical properties are influenced by its components such as cement, microsilica, aggregates, plasticizers, accelerators and fibers (Melby, 1994; Thomas 2009). Accelerators are particularly important in their selection as the use of SC in underground constructions requires the compliance with early age strength and the possibility of being employed in thick layers without the risk of detachments and movements (Prudencio, 1998).

The early-age strength of SC is frequently more important than its ultimate strength. The advance speed of tunnel operations is strongly influenced by the rate of development of early-age strength, since it determines, both in soft ground and weak rock, when the excavation face can proceed again. As a matter of fact, re-entry is mainly influenced by the tunnel drive progression to ensure the safety of personnel to continue development (Mohajerani et al., 2015). Re-entry times range from 2 to 4 hours, where the Unconfined Compressive Strength (UCS) of the SC reaches 1MPa (Clements, 2004; Concrete Institute of Australia, 2010), however, this value is not standardized and it can be also lower, if safety is ensured (see Rispin et al., 2009). Iwaki et al. (2001) empirically determined that an UCS of 0.5–1MPa should be an adequate strength for SC to protect against rock-fall, although the safe re-entry times, based on strength measurements, is still determined on project basis (Mohajerani et al., 2015).

Because coring should not take place until an UCS value of at least 5MPa (Clements, 2004), or between 8–10MPa, as Jolin and Beaupré (2003) suggest, the assessment of strength improvement is normally indirectly performed by means of the J-curves method for minimum strength (DIN EN 14487-1, 2006) by using the needle penetration method up to 1MPa strength (DIN EN 14488-2, 2006) and the stud driving method between 1 and 56 MPa strength (DIN EN 14488-2, 2006; ÖVBB, 2006). Conventional compressive strength tests on cored samples are only performed from UCS from 5 to 100MPa according to the DIN EN 12504-1 (2009).

After the SC application, with the restart of the tunnel excavation, the lining load phase starts. This loading phase occurs during the curing of the SC when the mechanical characteristics (strength and stiffness) vary over time at a certain rate. Each load step, due to each excavation face advance, produces different effects on the lining, due to the different stiffness and strength of the SC. The final tensional state and, therefore, the final conditions of the lining are the ultimate result of this complex loading mechanism due to the excavation face advance (while the SC cures) and the corresponding variations in its mechanical characteristics (Oreste, 2003).

The Converge Confinement Method (CCM) and the Hyperstatic Reaction Method (HRM) have been used in this paper to study in detail the behavior of the tunnel support under external loads with increasing elastic modulus values of SC simulating the curing effect. CCM generally requires a mean stiffness of the SC lining to obtain the support reaction line (Oreste, 2003). In this research, the reaction line of the SC lining is considered as curve, in order to simulate the curing effect of the SC during the loading phase of the support. CCM was useful to evaluate the magnitude of the various loading steps developing over time during the excavation face advance. In the HRM the interaction between ground and support is represented by Winkler type springs. This method permits to determine the displacement of the lining and the developed bending moments and forces in order to design it (Oreste, 2007; Do et al. 2014a; 2014b). In the specific case, at the HRM model different loading steps, obtained with the CCM, have been applied, considering in each of these steps the effective stiffness value reached by the SC and hence by the support. Due to the results obtained with the combined analysis of the two calculation methods, it was possible to obtain a detailed evaluation of the stress state of the support, which

120 can consider both the effect of the characteristics of the SC employed (with the evolving curve of
121 strength and stiffness with time) and the advance rate of the excavation face.

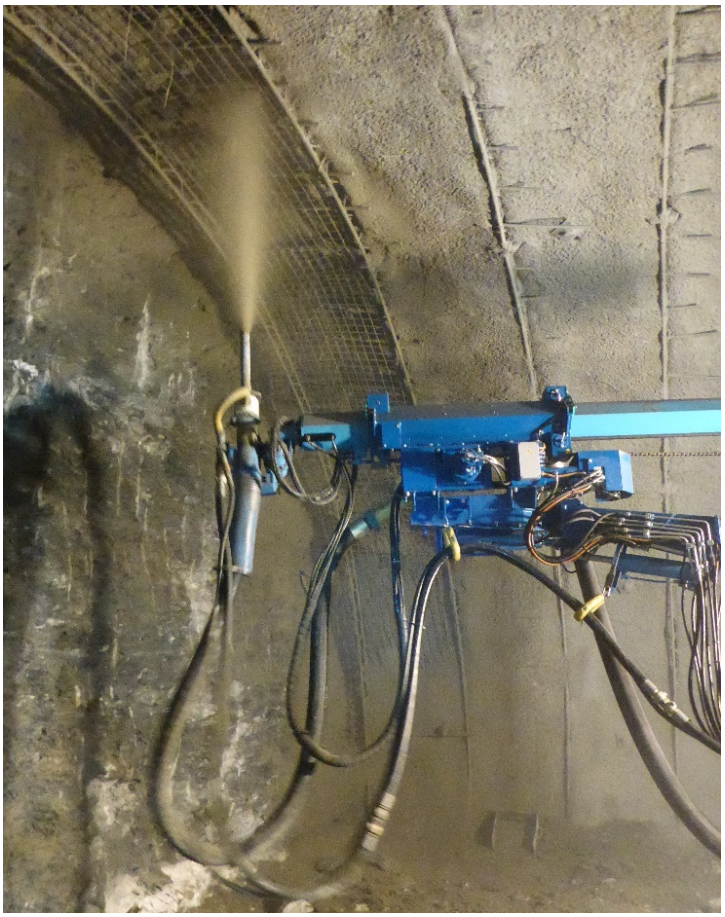

122

123 **Fig. 1 Spraying the tunnel roof with the shotcrete spraying machine (picture courtesy**
124 **Roland Mayr, BASF)**

125 **NUMERICAL MODEL**

126 The numerical procedure developed to obtain a detailed analysis of the stress and strain state of
127 a SC lining tunnel presented in this paper can be studied easily by a combined analysis of CCM
128 and HRM. The necessary calculation parameters are as follows: mechanical parameters of the
129 rock, tunnel radius, lithostatic stress state at the corresponding depth, lining thickness, evolving
130 curve of the strength and stiffness of the SC over the time, the advance rate of the excavation
131 face and the frequency and duration of the excavation operation stand still, to allow the support
132 installation and other operations on the site.

The CCM is based on the analysis of the stress and strain state that develops in the rock around a tunnel. The simplicity of the method is due to the important hypotheses on which it is based (e.g. Oreste, 2009; 2014; Spagnoli et al., 2017):

- Circular and deep tunnels (boundary conditions of the problem to infinity);
- Lithostatic stresses of a hydrostatic type and constant in the surrounding medium of the tunnel (the variation of the stresses with depth due to the weight of the rock is neglected);
- Continuous, homogeneous and isotropic rock mass;
- Bi-dimensional problem and plane stress field.

CCM consists of the definition of the convergence-confinement curve (CCC), that is the relationship between the internal pressure and the radial displacement $(p - |u|)$ on the boundary of the tunnel represented by a circular void (Oreste, 2009), see Fig. 2.

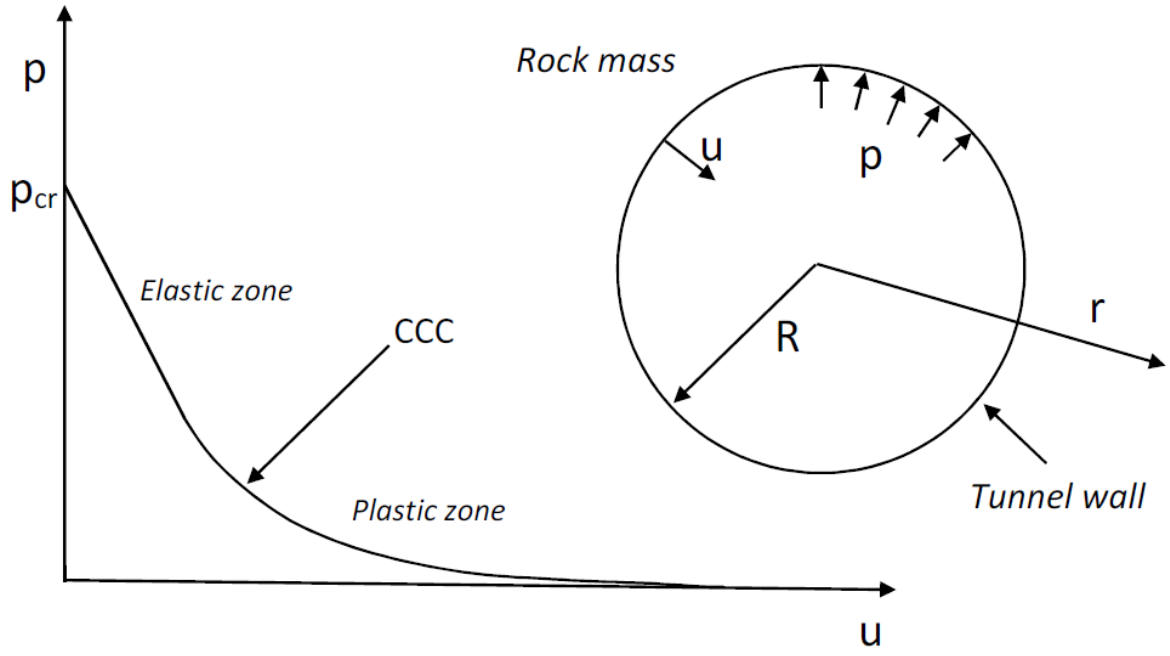

Fig. 2: Convergence-confinement method: Geometry of the problem and example of a convergence-confinement curve. Key: p: Internal tunnel pressure, R: Tunnel radius, r: Radial coordinate, u: Radial displacement of the tunnel wall, p_{cr}: Critical pressure (modified by Oreste, 2009).

Along with the CCC it is possible to draw on the same graph also the reaction line of the SC lining (RLSL). This reaction line starts from a point on the abscissa (where pressure in zero) but the displacement u^* is different from zero. The pressure p (the radial load on the lining,

corresponding also to the radial pressure applied by the lining on the tunnel wall) increases with increasing displacement u (the radial displacement of the tunnel wall). At the lining installation (initial point of the reaction line), the pressure applied at the extrados is zero, but a displacement of the tunnel wall, u^*, already occurred (Oreste, 2003). The reaction line is concave because the stiffness of the SC increases over the time, causing increased loads on the lining and reduced radial displacement of the tunnel wall (Oreste, 2003), see Fig. 3. The pressure difference at a certain displacement level u between the CCC and RLSL is called fictitious pressure (p_{fict}) and it is the static contribute of the excavation face on the investigated vertical section of the tunnel. The fictitious pressure can be evaluated as a function of the (positive) distance x between the investigated section and the excavation face, with the well-known equation of Panet and Guenot (1982):

$$p_{fict} = a \cdot p_0 \cdot \frac{b}{x+b} \quad (1)$$

Where: $a = 0.72$ and $b = 0.845 \cdot R$.

Starting from the initial point of the reaction line ($p = 0; u = u*$) and knowing the initial elastic modulus of the SC after the re-entry, it is possible to obtain the initial slope of the reaction line, k (Oreste, 2009) based on the support geometry (tunnel radius and thickness), the elastic modulus and the Poisson ratio, *v*, of the SC. Proceeding with a numerical approach, an initial segment of the RLSL for a small increase Δu of u is drawn. At the end of this first segment, p_{fict} can be evaluated as the difference between CCC and RLSL and from the fictitious pressure the distance x reached by the excavation face, using equation 1 (Fig. 3).

As excavation advance rate is known, and hence the relation linking x to the time, t, at each distance x reached by the excavation face with respect to the investigated section, a time value t corresponding subsequent to the SC lining installation can be given. At first load step Δp (evaluated as the difference from the final value and the initial value of p in the first segment of the RLSL) the reached time at the end of the first segment can be associated and therefore also the mean elastic modulus of the SC in the period corresponding to the initial linear part of RLSL. The method continues in the same way for successive small linear segments, until the intersection between the CCC and the RLSL is obtained. The intersection point between the two

curves represents the final stage of the loading process when the excavation face is advanced at a distance where static effects on the investigated vertical section of the tunnel are negligible (Fig. 3).

The procedure for the generic calculation step j is the following:

- Evaluation of the pressure p reached by the RLSL in the final point of the previous segment $p_{lin,j-1}$ and by difference between CCC and RLSL in such a point, evaluation of the fictitious pressure $p_{fict,j-1=}\, p_{j-1} - p_{lin,j-1}$, p_{j-1} is the pressure read on CCC in correspondence of the displacement u_{j-1} ;
- If the $p_{fict,j-1}$ is known, the corresponding distance x_{j-1} of the excavation face is calculated using equation 1;
- Knowing the face advance rate, the duration and frequency of still stands of the excavation phase, i.e. the relation $x = f(t)$, it is possible to determine the time t_{j-1} subsequent to the installation of the SC in the investigated section;
- If the evolving trend of the elastic modulus of the SC over the time is known, it is possible to determine the elastic modulus E_{j-1} and therefore the stiffness of the SC lining k_{j-1} in function of the time t_{j-1} ;
- The knowledge of the stiffness k_{j-1} allows to draw the new straight line of the RLSL for the step j for a predetermined amplitude of the radial displacement u equal to Δu; at the end of such a segment we obtain: $p_{lin,j=}\, p_{linj-1} + k_{j-1} \cdot \Delta u$;
- The difference $p_{lin,j-}\, p_{linj-1}$ is the loading step $\Delta p_{lin,j}$ of the step j, linked to the mean elastic modulus of the SC, $E_{,mean,j}$ in the step j where $E_{,mean,j} = 0.5(E_{j-1} + E_j)$.

Therefore, in the detailed study of the stress state in the SC lining, the knowledge of the evolving trend of the SC, $E = f(t)$, is fundamental. Generally, the variation of the UCS over the time, $\sigma_c = f(t)$, is evaluated. Then, the relation between the elastic modulus and UCS is considered constant over time. This is given by the equation of Chang (1993):

$$\sigma_{c,t} = \left(\frac{E_{,t}}{3.86}\right)^{1/0.6} \quad (2)$$

Where:

$E_{,t}$ is the SC elastic modulus at the time t;

206 $\sigma_{c,t}$ is the UCS for the SC at the time t.

207 A method to represent the variation of the elastic modulus over the time is given by Pottler
208 (1990):

$$E_{,t} = E_{,0} \cdot (1 - e^{-\alpha \cdot t}) \quad (3)$$

209 Where:

210 • $E_{,t}$ is the SC elastic modulus at the time t;

211 • $E_{,0}$ is the value of the asymptotic elastic modulus of the SC, for $t = \infty$;

212 • α is a time constant (t^{-1}).

213 From the practical point of view, UCS of SC is measured over the time subsequent to the lining
214 installation and from these values, a series of elastic modulus values for different times is
215 obtained.

216 Then the negative exponential curve, which best approximates these obtained points, i.e. the
217 pairs of values of the elastic modulus and the associated time, is obtained. This curve will have a
218 particular value of the asymptotic elastic modulus, $E_{,0}$, and of the coefficient α in equation 3.

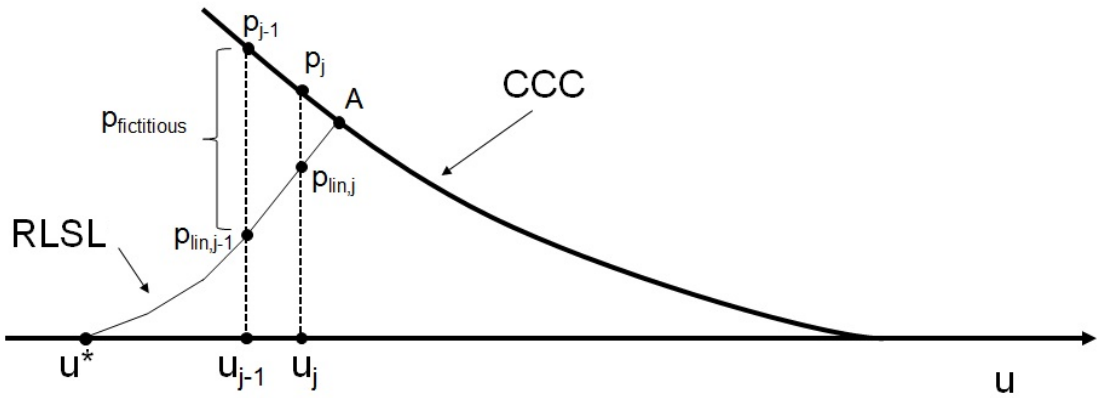

219

220 **Fig. 3 Convergence-confinement curve and reaction curve of the shotcrete lining with**
221 **numerical integration of the reaction curve of the shotcrete lining and a calculation step. A**
222 **is the interaction between reaction line and CCC to identify the final load process. Not to**
223 **scale.**

224 The analysis with HRM permits to evaluate in detail the behavior of SC (Oreste, 2007). In more
225 detail, it is possible to analyze the interaction between the SC lining and the surrounding rock
226 mass, during the loading phase of the support. This loading phase can take place gradually,
227 depending on the different load steps identified in the CCM analysis as outlined above. At each

load step, the stiffness value of SC lining is updated. HRM allows to obtain the exact course of the bending moment (*M*), the normal force (*N*) and the shear force (*T*) along the whole SC lining at each load step and at the end of the loading stage of the lining (in the final state when the excavation face is far from the investigated section). The knowledge of the values of *M*, *N*, and *T* allows to evaluate at each point of the lining the normal and the shear stresses that are developed, and thus also the safety factor against the SC failure. It is therefore possible to determine the minimum safety factor present along the SC lining, for each load step and at the end of the loading phase of the support. Very interesting is the determination of the safety factor over time: in this way, it is possible to check whether the SC lining has transient conditions in which the safety factor drops to lower values than the obtained final value. HRM is based on the finite element method (FEM) and consists in dividing the SC lining of the tunnel into one-dimensional elements. These elements have axial and flexural stiffness and are therefore able to develop axial displacements, lateral displacements and rotations at their ends. The one-dimensional elements are interconnected in succession through nodes. At each node, Winkler springs are applied in both perpendicular and tangential direction to the lining. These springs allow to simulate the interaction between the lining and the rock wall.

From the local stiffness matrix of each element it is possible to come to the definition of the overall stiffness matrix of the lining. In this paper only half of the lining was considered, for symmetry reasons with respect to the vertical axis passing through the center of the tunnel. The elements considered are 36, therefore the total number of nodes is 37. The global stiffness matrix K is given by the following expression:

$$K = \begin{bmatrix} k_{1,a} & k_{1,b} & 0 & 0 & 0 & \cdots & 0 \\ k_{1,c} & k_{1,d}+k_{2,a} & k_{2,b} & 0 & 0 & \cdots & 0 \\ 0 & k_{2,c} & k_{2,d}+k_{3,a} & k_{3,b} & 0 & \cdots & 0 \\ 0 & 0 & k_{3,c} & k_{3,d}+k_{4,a} & \ddots & \cdots & 0 \\ 0 & 0 & 0 & \ddots & \ddots & \ddots & 0 \\ \vdots & \vdots & \vdots & \vdots & \ddots & \ddots & k_{i,b} \\ 0 & 0 & 0 & 0 & 0 & k_{i,c} & k_{i,d} \end{bmatrix} \quad (4)$$

where the terms $k_{i,a}$, $k_{i,b}$, $k_{i,c}$, $k_{i,d}$ represent the 3x3 sub-matrices of the local k_i stiffness matrix of the ith one-dimensional element of the SC lining:

$$k_i = \begin{bmatrix} \frac{EA}{I}c^2+\frac{12EJ_z}{I^3}s^2 & \frac{EA}{I}c^2-\frac{12EJ_z}{I^3}s^2 & -\frac{6EJ_z}{I^2}s & -\frac{EA}{I}c^2-\frac{12EJ_z}{I^3}s^2 & -\frac{EA}{I}c^2+\frac{12EJ_z}{I^3}s^2 & -\frac{6EJ_z}{I^2}s \\ \frac{EA}{I}cs-\frac{12EJ_z}{I^3}cs & \frac{EA}{I}s^2+\frac{12EJ_z}{I^3}c^2 & \frac{6EJ_z}{I^2}c & -\frac{EA}{I}cs+\frac{12EJ_z}{I^3}cs & -\frac{EA}{I}s^2-\frac{12EJ_z}{I^3}c^2 & \frac{6EJ_z}{I^2}c \\ -\frac{6EJ_z}{I^2}s & \frac{6EJ_z}{I^2}c & \frac{4EJ_z}{I} & \frac{6EJ_z}{I^2}s & -\frac{6EJ_z}{I^2}c & \frac{2EJ_z}{I} \\ -\frac{EA}{I}c^2-\frac{12EJ_z}{I^3}s^2 & -\frac{EA}{I}cs+\frac{12EJ_z}{I^3}cs & \frac{6EJ_z}{I^2}s & \frac{EA}{I}c^2+\frac{12EJ_z}{I^3}s^2 & \frac{EA}{I}cs-\frac{12EJ_z}{I^3}cs & \frac{6EJ_z}{I^2}s \\ -\frac{EA}{I}cs+\frac{12EJ_z}{I^3}cs & -\frac{EA}{I}s^2-\frac{12EJ_z}{I^3}c^2 & -\frac{6EJ_z}{I^2}c & \frac{EA}{I}cs-\frac{12EJ_z}{I^3}cs & \frac{EA}{I}s^2+\frac{12EJ_z}{I^3}c^2 & -\frac{6EJ_z}{I^2}c \\ -\frac{6EJ_z}{I^2}s & \frac{6EJ_z}{I^2}c & \frac{2EJ_z}{I} & \frac{6EJ_z}{I^2}s & -\frac{6EJ_z}{I^2}c & \frac{4EJ_z}{I} \end{bmatrix} \quad (5)$$

$c = \cos\alpha_i \quad s = \sin\alpha_i$

where α_i is the angle of inclination of the element ith with respect to the horizontal; E is the elastic modulus of SC lining, *A* the area of the lining section, *J* the moment of inertia of the lining section, *l* is the length of the one-dimensional element.

$[k_{i,a}], [k_{i,b}], [k_{i,c}], [k_{i,a}]$ are thus positioned within the local stiffness matrix k_i :

$$[k]_i = \begin{bmatrix} k_{i,a} & k_{i,b} \\ k_{i,c} & k_{i,a} \end{bmatrix} \quad (6)$$

The elements of a diagonal band of the global stiffness matrix (equation 4) are then modified to add the values of the normal and tangential stiffness of the springs simulating the interaction of the SC lining with the rock wall (Oreste, 2007).

Once the global stiffness matrix *K* is defined, and knowing the vector of the nodal forces $\{F\}$ applied to the numerical model (i.e. the external loads applied to the lining), it is possible to determine the vector of nodal displacements $\{S\}$ from the following relation:

$$[K] \cdot \{S\} = \{F\} \quad (7)$$

From the vector of the nodal displacements, it is possible to obtain the radial displacements of the lining, which give indications of its global deformation and also of the interactions with the rock wall. From the nodal displacements, it is also possible to obtain the normal force N, the shear force T and the bending moment M. From these stress characteristics, it is possible to define in detail the existing stress state in the lining and, therefore, also the factor of safety that the lining reaches for each load step and over time.

For each load step of the lining, the global stiffness matrix as function of the elastic modulus of SC reached for the specific load step is evaluated. The load step is used in order to determine the

nodal forces for each step. The vector of the nodal displacements obtained for each load step will update the total displacements achieved; the values of *M*, *N*, *T* and the normal tangential stresses obtained for each load step update the corresponding overall values achieved. The final situation is represented by the total displacements and total stresses, as the sum of the values obtained for each step of loading.

NUMERICAL RESULTS AND DISCUSSION

The calculation procedure proposed in this article has been applied to some examples, in order to verify which can be the effect on the stress state in the SC lining, by varying the characteristics of the SC (in particular the curing rate and final elastic modulus) and the advance rate of the excavation face.

Different geometries of the tunnel were considered, along with various rock mass types. In general, six main examples are presented, each of which has four cases. The cases considered include the following assumptions, in accordance with the underlying hypotheses of the calculation methods which were used in the procedure presented.

- a bi-dimensional stress state considering circular and deep tunnels;
- a continuous, homogeneous and isotropic rock mass.

The first example (example 1) refers to a tunnel of 2m radius excavated in a rock of poor quality. The geomechanical parameters are shown in Tab. 1. The lithostatic stress p_0 is 7MPa and the fictitious internal pressure p_{fict} at the face is $0.72 \cdot p_0$, where the SC lining is installed. SC lining has a thickness of 20cm. The horizontal stress in the lithostatic environment is ½ of the vertical one (K_0 =0.5).

Rock Mass Parameters	
Elastic modulus [MPa]	3160
Poisson‘s ratio	0.30
Peak cohesion [MPa]	0.15
Residual cohesion [MPa]	0.12
Peak angle of friction [°]	20
Residual angle of friction [°]	16
Dilatancy [°]	16

Table 1. Geomechanical parameters for the rock mass for example 1

Since the calculation procedure uses HRM, the values of the stiffness of the interaction springs of the support with the ground are obtained by the following expressions:

$$K_n = 2 \cdot \frac{E_{rm}}{R} \cdot b \quad (8)$$

$$K_s = \frac{K_n}{2} \quad (9)$$

Where: $b = 2 \cdot R \cdot cos(2{,}5°) \cdot sin(2{,}5°)$, R and $E_{rm}$is the elastic modulus of the rock mass. Two different types of SC were assumed with a final and asymptotic value of the elastic modulus ($E_{,0}$) of 6000 and 12000MPa, both with a Poisson's ratio, *v*, 0.15. The time constant α has a value of 0.05 h^{-1} in both cases (eq. 3). The diagrams relating the modulus of elasticity and UCS varying with time are shown in Fig. 4.

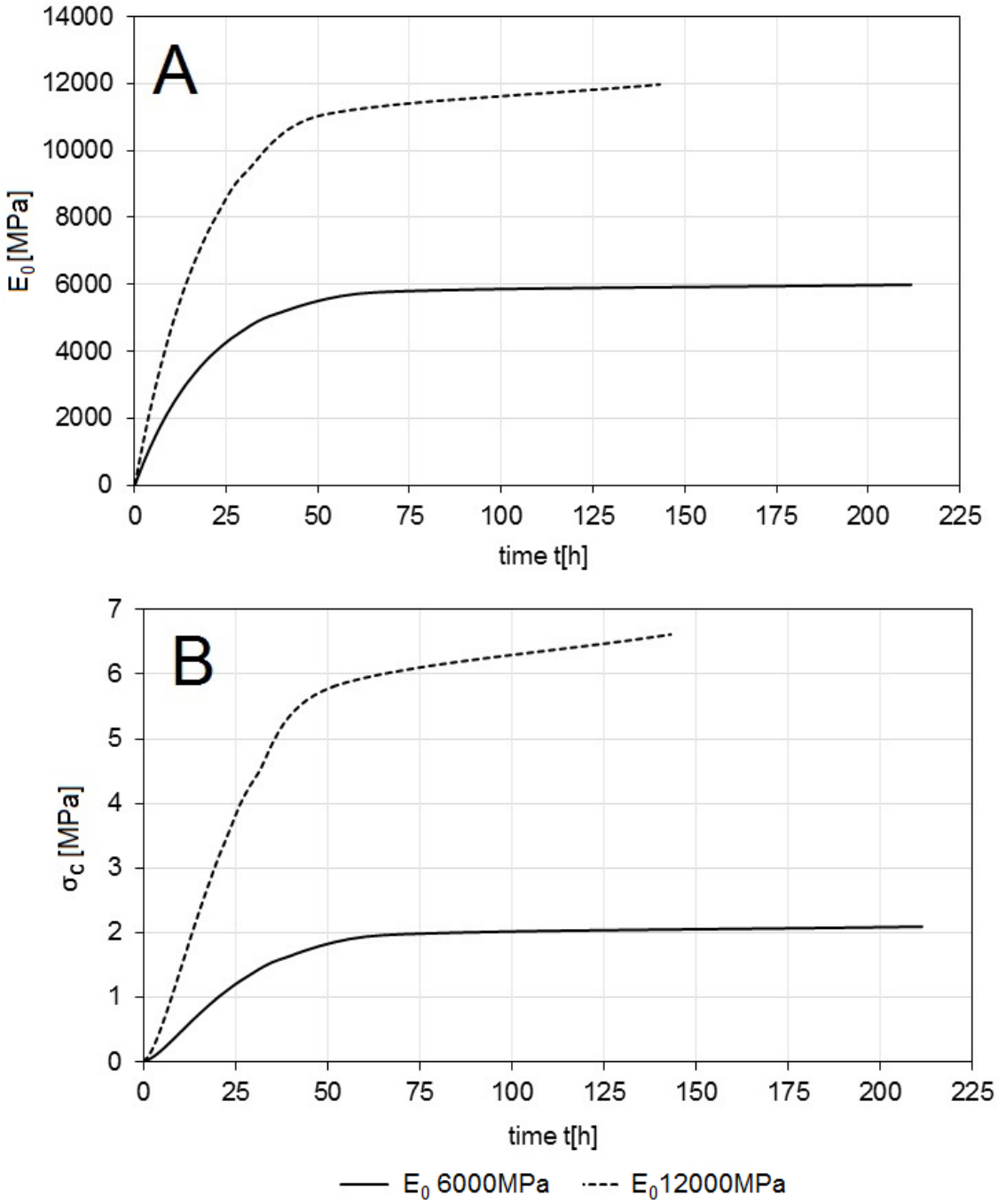

Fig. 4 Progressive increase of the asymptotic elastic modulus (A) and UCS (B) of the shotcrete with time for the two considered typologies in the example 1.

The other parameter to be varied is the daily mean rate of tunnel advance (assumed as 2 m/day and 10m/day), with support installation time t_0 and the advance step δ equal to 1h and 1.2m, respectively.

The reaction lines of the SC linings are shown in Fig. 5 for the four analyzed cases.

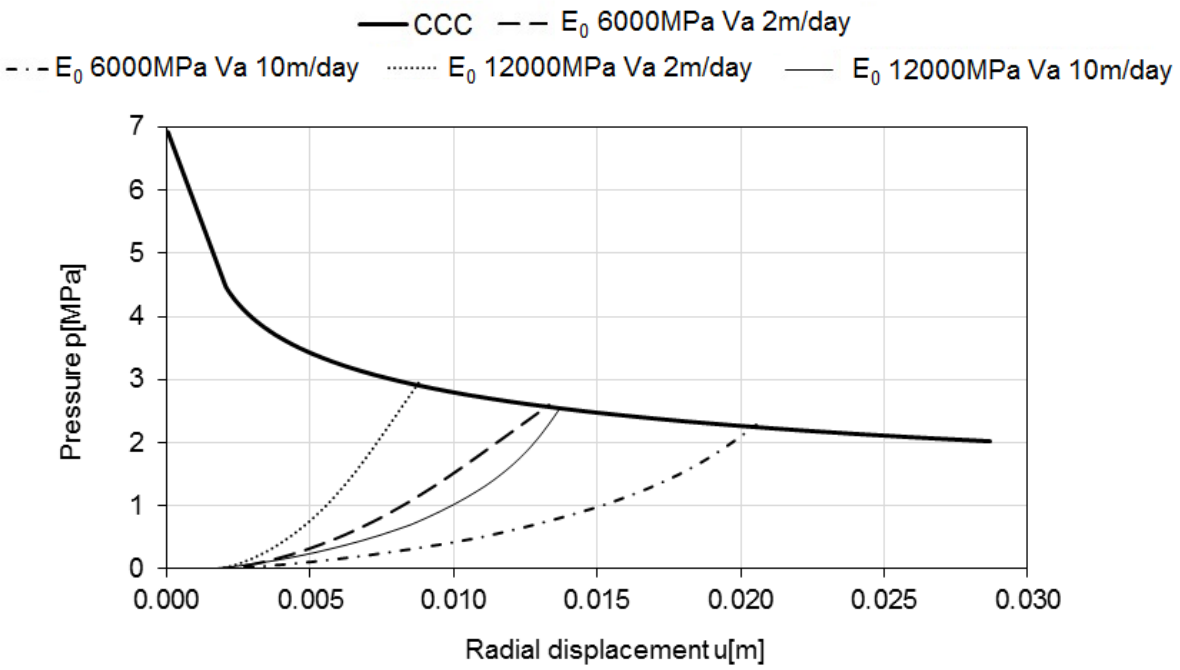

Fig. 5 Reaction curves of the SC lining as a function of the face advance rate (Va) and the mechanical characteristics of the shotcrete for the example 1.

It is possible to see in Fig. 5 the change of the equilibrium point (intersection between the CCC and the SCRL) for each of the cases. In addition, it can be observed that the reaction line is not straight but curved. This is because the calculation model considers the curing time of the SC, i.e. the progressive increase of the modulus of elasticity and UCS from the installation of the support to the point at which the maximum asymptotic strength and stiffness of the SC has been obtained.

The influence of the SC type and advance rate (Va) appears to be very important in the final evaluation of the equilibrium point and, hence, of the final loading on the SC lining and the final displacement of the tunnel wall.

The final load on the lining, as well as the final displacement of the tunnel wall, may vary significantly depending on the type of SC used and the tunnel face advancing speed. The highest final stress values are found for the most rigid type of SC and the lowest advance rate.

Also the stress and displacement characteristics of the lining can vary significantly. In the following the values referring to the final condition (at the equilibrium point) for example 1 are shown (Fig. 6).

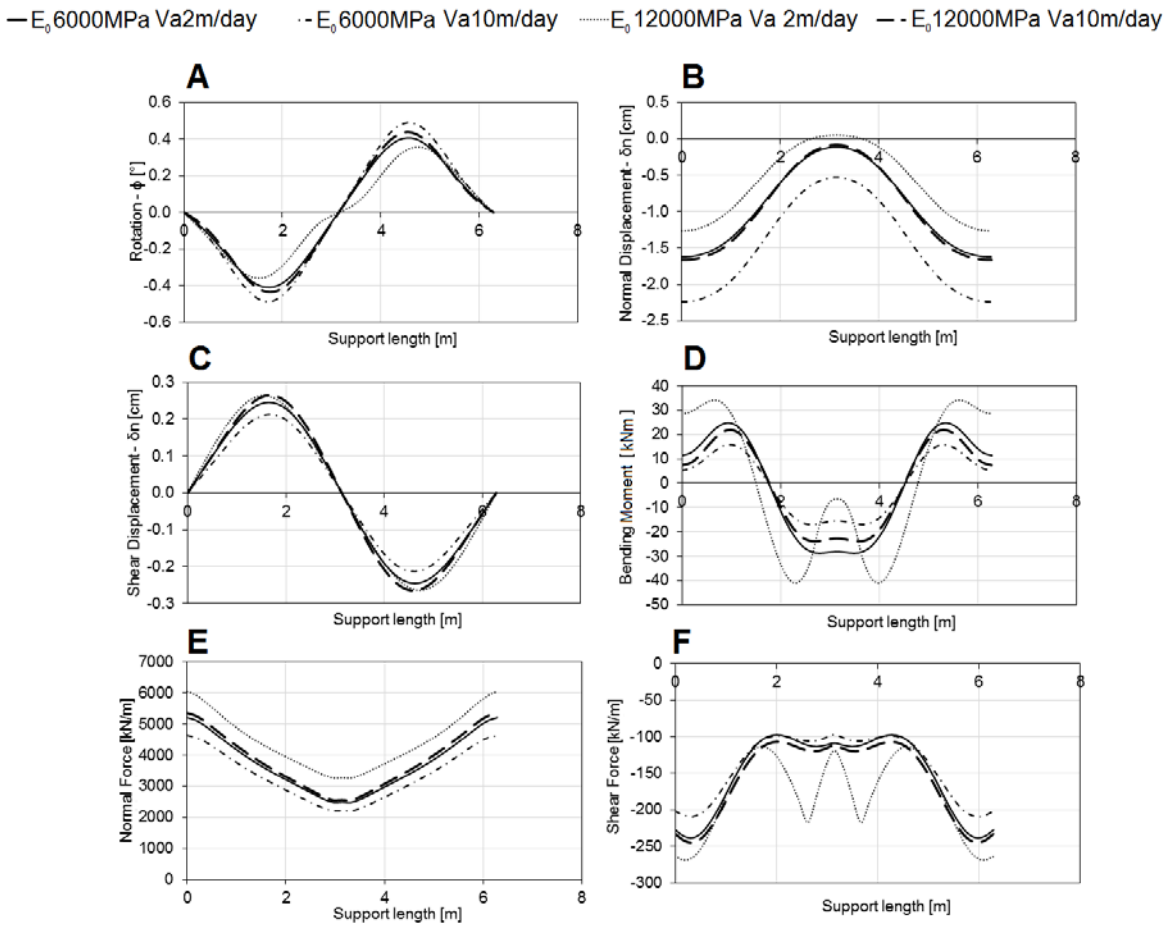

325

326 **Fig. 6 Variation of the rotation (A), normal displacement (B), shear displacement (C),**
327 **bending moment (D), normal force (E) and shear force (F) for the two considered type of**
328 **SC and two assumed advance rates (Va) of the tunnel face, with reference to the final**
329 **equilibrium point (example 1).**

330 Of particular interest is the trend of normal displacements, bending moments, normal and shear
331 forces along the lining (i.e. length of the beam elements considered for the calculation). Lower
332 stiffness during the concrete setting period and faster advance speed provide larger normal
333 displacements. Conversely, higher stiffness and lower advance rate produce lower normal
334 displacements. The highest peak moments are detected in the lining when using high stiffness
335 SC and low advance speed. The opposite is for lower stiffness and higher advance speed. Same
336 considerations can be made for normal and shear forces.

337 In the example 2 a tunnel with a radius R of 2.5m, excavated in a rock with poor mechanical
338 properties (RMR=40, see Tab. 2), is considered. The lithostatic pressure p_0 is 5MPa. Also in this
339 example, the lining thickness is 20cm and K_0 is 0.5.

Rock Mass Parameters	
Elastic modulus [MPa]	21170
Poisson‘s ratio	0.30
Peak cohesion [MPa]	1.5
Residual cohesion [MPa]	1.5
Peak angle of friction [°]	33
Residual angle of friction [°]	33
Dilatancy [°]	16

Table 2. Geomechanical parameters for the rock mass in the example 2

Four different cases were analyzed in which higher final elastic modulus values of the support ($E_{,0}$) were taken as 12000 and 28000MPa. The α time constant has a value of 0.05 h^{-1} and the Poisson‘s ratio *v* of 0.15. The tunnel advance daily rates were arbitrary assumed to be 4 m/day and 12 m/day, with support installation time t_0 and the advance step δ of 1 h and 1.2 m respectively. The different reaction lines of the SC lining in conjunction with the CCCs are presented in Fig. 7, where it is possible to identify the equilibrium point corresponding to each analyzed case.

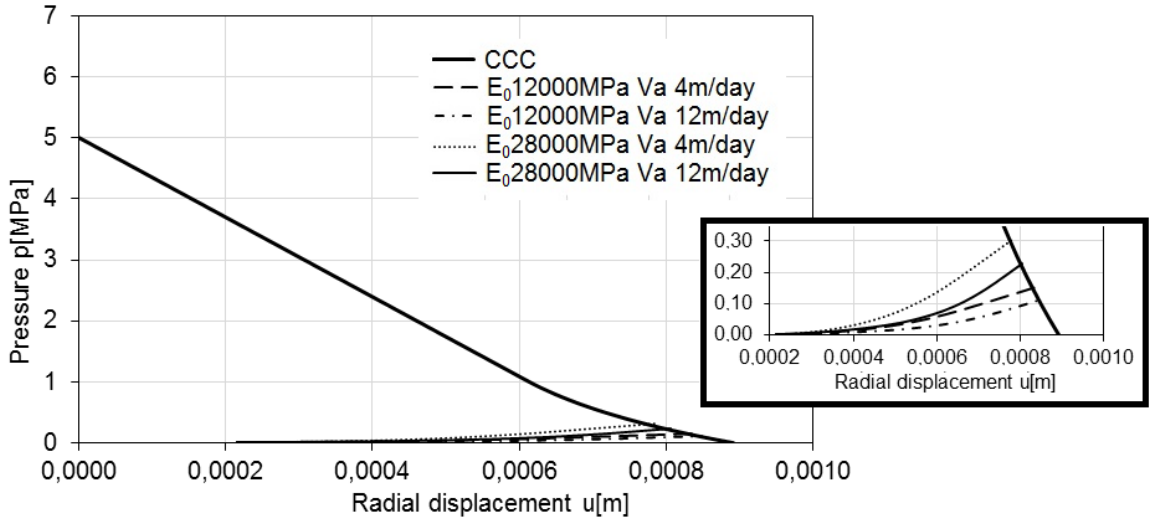

Fig. 7 Reaction curve of the shotcrete lining (with enlargement on the right side) as a function of the face advance rate (Va) and the shotcrete type considered in the example 2.

In this second example, lower final pressures are observed on the lining, but the differences between the 4 cases considered are in very high percentages. Higher final pressures have a higher final elastic modulus and a lower advance rate.

The results in terms of displacements and stress characteristics along the lining circumference for the four cases presented in this example, when the final condition is reached, are shown in Fig. 8.

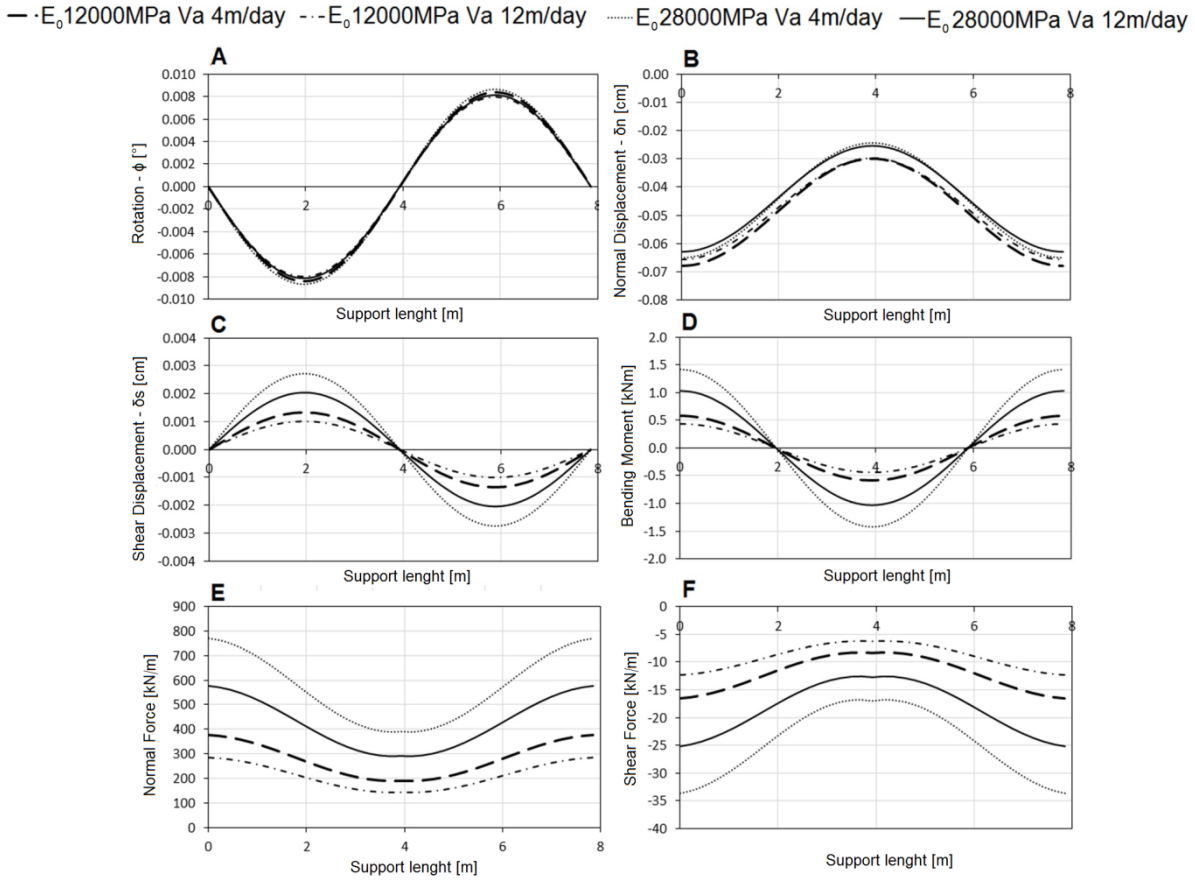

Fig. 8 Variation of the rotation (A), normal displacement (B), shear displacement (C), bending moment (D), normal force (E) and shear force (F) for the two considered types of SC and two assumed velocities of advance (Va) of the tunnel face, with reference to the final equilibrium point (example 2).

Examples 3 and 4 refer to two tunnels built on rock with the same characteristics, differing from one another only in size. Examples three and four were analyzed in four different cases, in which the elastic modulus values of SC were obtained by the UCS values given in Melbye (1994). The first proposed SC installation was implemented in the tunnel of Blisadona (Austria) where a final value of elastic modulus of 30000MPa was calculated based on equation 2. The second is a SC installed in a tunnel located at Quarry Bay Station (Hong Kong) where a final value of elastic modulus of 42000MPa was calculated. The time constant α (equation 3) and the Poisson's ratio v of the SC were assumed to be 0.05 h^{-1} and 0.15 respectively. The mechanical properties of the rock mass arbitrary assumed for these examples are shown in Tab. 3. For the example 3 a radius of 2m has been assumed, while for the example 4 a larger dimension with a radius of 7m has

been hypothesized. The in situ hydrostatic stress p_0 was assumed as 7MPa, with a SC lining thickness of 20cm and K_0 value of 0.5. The daily advance rates were arbitrary assumed for both examples 2m/day and 6m/day, with installation time of the support t_0 equal to 6h and the advance step δ of 3.5m.

Rock Mass Parameters	
Elastic modulus [MPa]	21170
Poisson‘s ratio	0.30
Peak cohesion [MPa]	1.5
Residual cohesion [MPa]	1.5
Peak angle of friction [°]	33
Residual angle of friction [°]	33
Dilatancy [°]	16

Table 3. Geomechanical parameters for the rock mass for example 3 and 4

In Fig. 9 the reaction lines of the SC lining for the four considered cases are shown. It is worth noticing as for the example of the smallest tunnel (example 3), considering all the other parameters being equal in the calculation, the differences in terms of final load on the lining and final tunnel wall displacement are more pronounced. In the case of a large tunnel (example 4), the differences between the 4 cases examined are smaller.

However, even in these two calculation examples it is noted that the major final pressures are observed for the lining with a higher stiffness and with lower face advance rate.

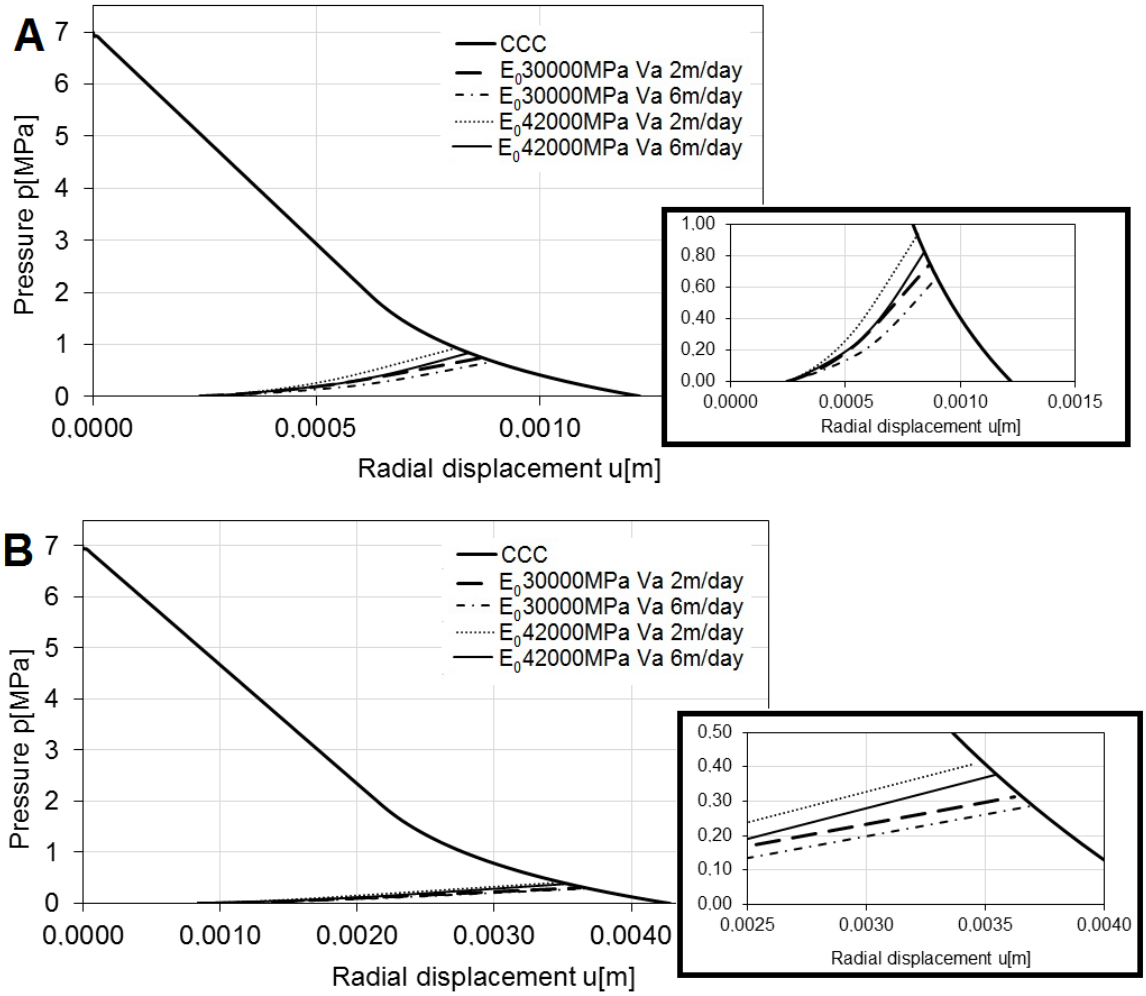

383

384 **Fig. 9 CCCs and reaction curve of the shotcrete lining (with enlargement on the right side)**

385 **as a function of the velocity of advance (Va) and the final elastic modulus of the shotcrete,**

386 **for example 3 (A) and example 4 (B).**

387 Displacements and stress characteristics along the lining are shown in Figs. 10 and 11.

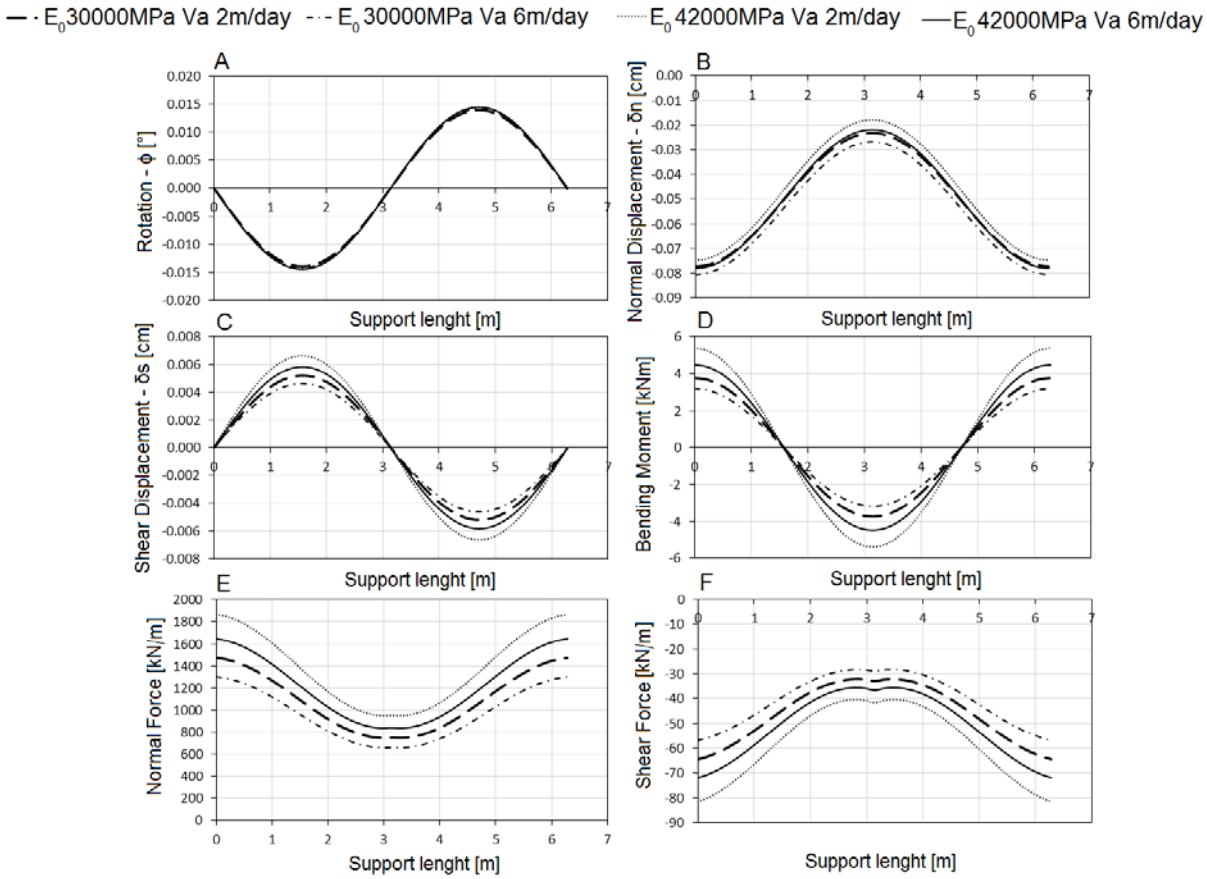

388

389 **Fig. 10 Variation of the rotation (A), normal displacement (B), shear displacement (C),**
390 **bending moment (D), normal force (E) and shear force (F) for two considered types of SC**
391 **and two assumed velocities of advance (Va) of the tunnel face, with reference to the final**
392 **equilibrium point (example 3).**

393 ϕ

394 δ

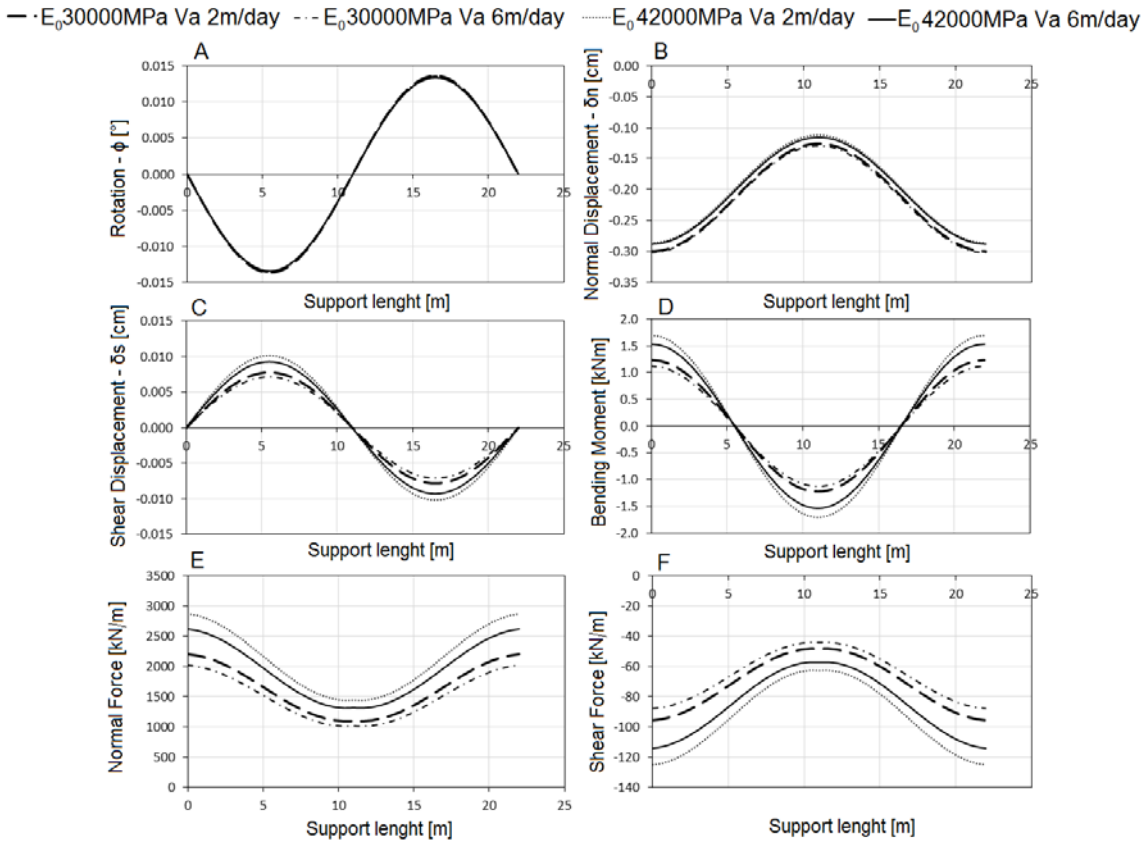

Fig. 11 Variation of the rotation (A), normal displacement (B), shear displacement (C), bending moment (D), normal force (E) and shear force (F) for the two considered types of SC and two assumed velocities of advance (Va) of the tunnel face, with reference to the final equilibrium point (example 4).

Even for these two examples, higher stress characteristics are observed for SC with higher stiffness during the concrete setting time and lower face advance rates. Major changes in terms of percentage occur among the four cases analyzed for the smaller tunnel, compared to the larger tunnel example.

Examples 5 and 6 refer to two tunnels of radius 2m and 7m, respectively, excavated in a rock mass with the same characteristics. The rock in these two examples, unlike the previous two, is a rock mass of good mechanical properties corresponding to RMR = 80. The geomechanical parameters are listed in Tab. 4.

The lithostatic pressure p_0 is assumed to be 7MPa, the SC lining has a thickness of 20cm and K_0 is equal to 0.5 for both examples. The daily advance rates and the SC types implemented in the support of these two examples are assumed to be the same types as in examples 3 and 4. The reaction lines of the SC lining in conjunction with the CCCs are shown in Fig. 12.

Rock Mass Parameters	
Elastic modulus [MPa]	57500
Poisson's ratio	0.30
Peak cohesion [MPa]	3.75
Residual cohesion [MPa]	3.75
Peak angle of friction [°]	42
Residual angle of friction [°]	42
Dilatancy [°]	16

Table 4. Geomechanical parameters of the rock mass in the example 5 and 6.

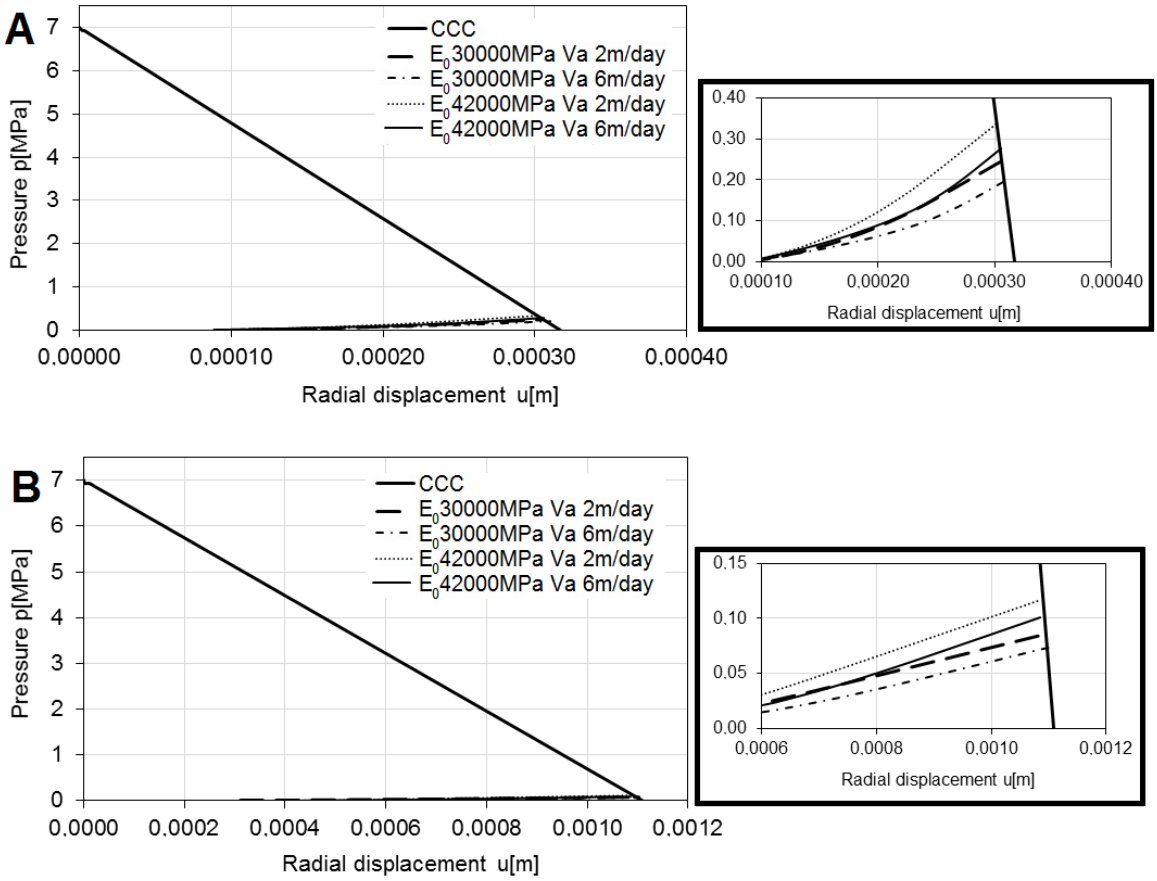

Fig. 12 CCCs of the tunnel and reaction lines of the shotcrete lining (with enlargement on the right side) as a function of the face velocity of advance (Va) and the shotcrete types for the example 5 (A) and 6 (B).

The stress characteristics (*M*, *N* and *F*) to determine the stress state in the lining and the more important displacements of the SC lining are shown in the Figs. 13 and 14.

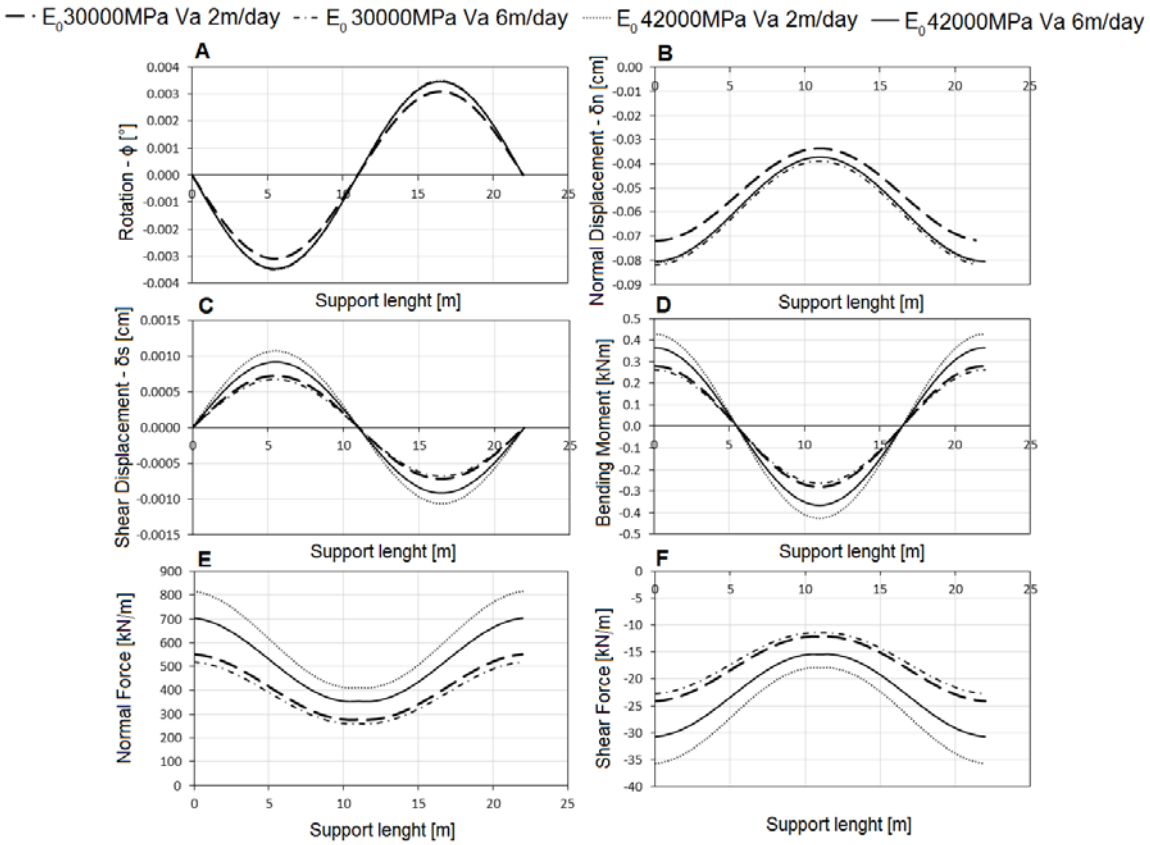

420

421 **Fig. 13 Variation of the rotation (A), normal displacement (B), shear displacement (C),**
422 **bending moment (D), normal force (E) and shear force (F) for the two considered types of**
423 **SC and two assumed velocities of advance (Va) of the tunnel face, with reference to the**
424 **final equilibrium point (example 5).**

425

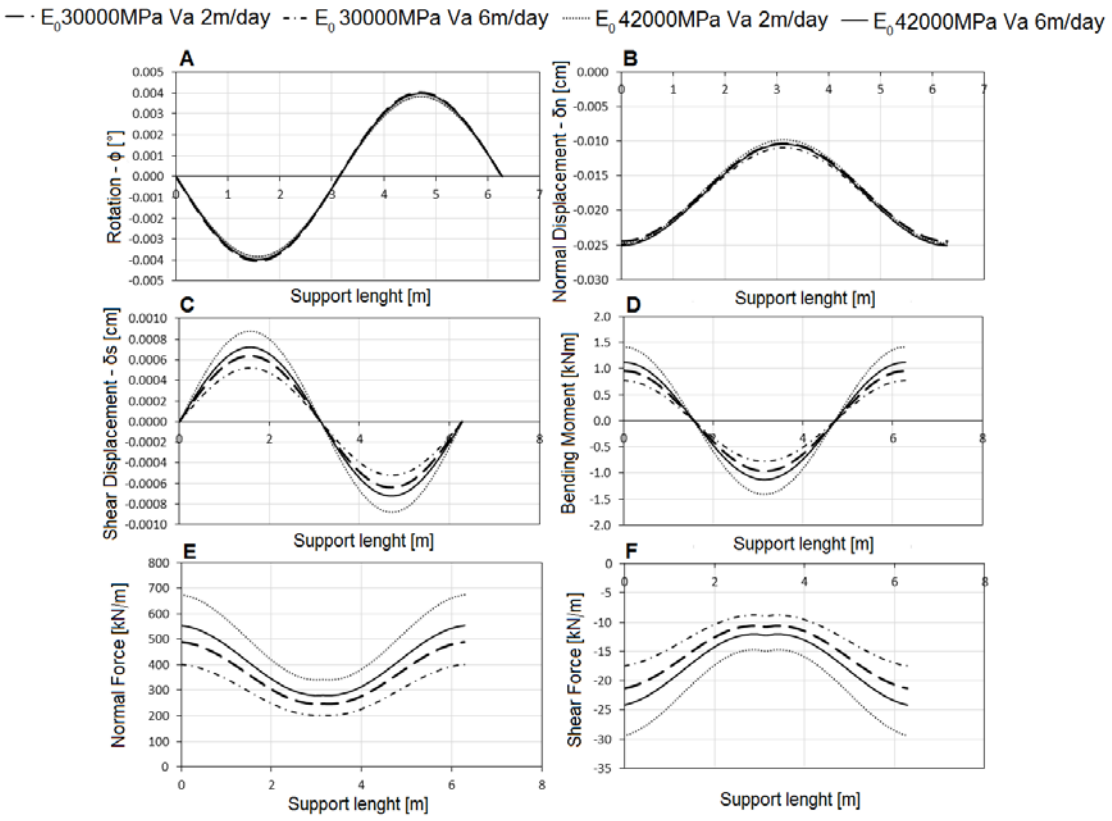

Fig. 14 Variation of the rotation (A), normal displacement (B), shear displacement (C), bending moment (D), normal force (E) and shear force (F) for the two considered types of SC and two assumed velocities of advance (Va) of the tunnel face, with reference to the final equilibrium point (example 6).

In high-quality rock masses, such as those for example 5 and 6, the final load on the lining is of low magnitude. In fact, the intersection between the CCC and the RLSL is for low pressure values. In the example 6 (R = 7m) there are no noticeable differences in the RLSL performance for the four examined cases, but there are some differences in example 5 (R = 2m).

On the other hand, the differences between the bending moments and the forces that develop inside the lining are more pronounced. The same considerations done previously are also here valid. In percentage terms, the variations found in the four examined cases are higher for example 5 (R = 2m) than for example 6 (R = 7m). In addition, for R = 7m and final elastic modulus of SC of 30GPa (lower stiffness between the two types of concrete used), the advance rate appears to have a minor influence on the trend of bending moments, normal and shear forces developed in the lining.

CONCLUSIONS

The sprayed concrete (shotcrete) linings represent one of the most popular tunnel supporting works. Its operating mechanism is quite complex due to the installation method, the particular load application phase and the SC curing with the consequent modification of the mechanical properties of the SC over time. Precisely because of the complexity of the operation of this support work, it is difficult to analyze the behavior and to evaluate its static conditions. The three-dimensional numerical analysis, able to consider all the complex aspects of the operating mechanism, requires very long calculation times.

In this article, after highlighting the fundamental characteristics of the SC, a new calculation procedure based on the combined use of two widely used calculation methods for tunnel linings was introduced: the Convergence-Confinement Method (CCM) and the Hyperstatic Reaction Method (HRM).

The former, thanks to the evaluation of the sprayed concrete reaction line (RLSL) and the intersection of the Convergence Containment Curve (CCC), allows obtaining the final load on the support and the evolution of the load with the progress of the curing phase of the SC. The latter, based on the results obtained with the former, allows determining the mechanical behavior of the lining and the interaction with the tunnel wall with the progress of the applied load and the development of mechanical parameters of the SC over time.

The interesting result is the trend of bending moments, normal and shear forces, and displacement along the lining circumference during the transient loading phase and in the final load condition.

From the stress characteristics, it is possible to assess the stress state in the SC and the safety factors of the lining against compression or traction failure in the SC. Note that the safety factors allow to correctly design the lining, defining in particular the average of the tunnel lining thickness.

The calculation procedure was then applied to examples, differentiated by the tunnel geometry and the geomechanical quality of the surrounding rock mass. For each example, four different cases were considered, taking into account two different types of SC and two different advance rates of the tunnel excavation face. From the results, it was possible to develop useful considerations on the parameters that mostly influence the mechanical behavior of the lining.

Thanks to the fact that the model is able to appropriately consider the evolution of the mechanical properties of SC over time and the advance rate of the excavation face, it is a useful tool for selecting two key parameters in a tunnel design, as the type of SC and the thickness of the lining.

REFERENCES

Chang, Y., and Stille, H. 1993. Influence of early age properties of shotcrete on tunnel construction sequences, in Wood, D.F., Morgan, D.R. (Eds.), Shotcrete for Underground Support VI, American Society of Civil Engineers, Reston, pp. 110-117.

Clements, M., 2004. Comparison of methods for early age strength testing of sprayed fibre reinforced concrete. In: Bernard, E.S. (Ed.), Proceedings of the 2nd International Conference on Engineering Developments in Sprayed Fibre Reinforced Concrete, Cairns, Queensland, Australia. Taylor and Francis Group, London, pp. 81–87.

Concrete Institute of Australia, 2010. Shotcrete in Australia. Concrete Institute of Australia, Rhodes, Australia.

DIN 18551 1992. Spritzbeton - Nationale Anwendungsregeln zur Reihe DIN EN 14487 und Regeln für die Bemessung von Spritzbetonkonstruktionen. Deutsches Institut fur Normung, e.V.

DIN EN 14487-1 2006. Spritzbeton - Teil 1: Begriffe, Festlegungen und Konformität. Deutsches Institut fur Normung, e.V.

DIN EN 14488-2 2006. Prüfung von Spritzbeton - Teil 2: Druckfestigkeit von jungem Spritzbeton. Deutsches Institut fur Normung, e.V.

DIN EN 12504-1 2009. Prüfung von Beton in Bauwerken - Teil 1: Bohrkernproben - Herstellung, Untersuchung und Prüfung der Druckfestigkeit. Deutsches Institut fur Normung, e.V.

Do, N.A., Dias, D., Oreste, P., and Djeran-Maigre, I., 2014a. The behavior of the segmental tunnel lining studied by the hyperstatic reaction method. Eur. J. Environmental Civil Eng. 18(4), 489–510.

Do, N.A., Dias, D., Oreste, P., and Djeran-Maigre, I., 2014b. A new numerical approach to the hyperstatic reaction method for segmental tunnel linings. Int. J. Numer. Anal. Meth. Geomech., 38, 1617–1632.

Franzen T, Garshol KF, and Tomisawa N (2001) Sprayed concrete for final lining: ITA working group report. Tunn. Undergr. Space Technol. 16:295–309.

Hemphill, G.B., 2013. Practical tunnel construction. John Wiley & Sons, Hoboken.

Iwaki, K., Hirama, A., Mitani, K., Kaise, S., and Nakagawa, K., 2001. A quality control method for shotcrete strength by pneumatic pin penetration test. NDT and E International, 34(6), 395-402.

Jolin, M., and Beaupré, D., 2003. Understanding Wet-Mix Shotcrete: Mix Design, Specifications, and Placement. American Shotcrete Association, 6-12.

Melbye, T. 1994. Sprayed Concrete for Rock Support. MBT International Underground Construction Group, Zürich.

Mohajerani, A., Rodrigues, D, Ricciuti, C., and Wilson, C., 2015. Early-Age Strength Measurement of Shotcrete. Journal of Materials, 2015 (ID 470160), http://dx.doi.org/10.1155/2015/470160

ÖVBB 2006. Guideline Sprayed Concrete. Österreichische Bautechnik Vereinigung.

Oreste P. 2003., Procedure for Determining the Reaction Curve of Shotcrete Lining Considering Transient Conditions. Rock Mech. Rock Eng. 36 (3), 209–236, DOI 10.1007/s00603-002-0043-z.

Oreste P. 2007, A numerical approach to the hyperstatic reaction method for the dimensioning of tunnel supports. Tunn. Undergr. Sp. Tech., 22, 185–205.

Oreste P. 2009, The Convergence-Confinement Method: Roles and limits in modern geomechanical tunnel design. American Journal of Applied Sciences 6(4), 757-771.

Oreste P. 2014, The Determination of the tunnel structure loads through the analysis of the Interaction between the void and the support using the convergence-confinement method. American Journal of Applied Sciences, 11(11), 1945.1954.

Oreste P., Spagnoli G., Luna Ramos C.A., and Sebille L. 2018. The Hyperstatic Reaction Method for the Analysis of the Sprayed Concrete Linings Behavior in Tunneling. Geotechnical and Geological Engineering, 36, 4, 2143-2169, *https://doi.org/10.1007/s10706-018-0454-6*.

Panet, M., and Guenot, A. 1982, Analysis of convergence behind the face of a tunnel. Proc. Tunnelling 82, Brighton, 197–204.

Pottler, R. 1990, Time-dependent rock-shotcrete interaction. A numerical shortcut. Comput. Geotechn. 9, 149–169.

Prudencio, L.R., 1998. Accelerating admixtures for shotcrete. Cement and Concrete Composites 20: 213-219.

Rispin, M., Howard, D., Kleven, O. B., Garshol, K., and Gelson, J., 2009. Safer, Deeper, Faster: Sprayed Concrete—An Integral Component of Development Mining, Australian Centre for Geomechanics.

Spagnoli, G, Oreste, P, and Lo Bianco, L. 2017. Estimation of Shaft Radial Displacement beyond the Excavation Bottom before Installation of Permanent Lining in Nondilatant Weak Rocks with a Novel Formulation. Int. J. Geomechanics, 17, 04017051 https://doi.org/10.1061/(ASCE)GM.1943-5622.0000949.

Thomas, A. 2009, Sprayed concrete lined tunnel. Taylor & Francis, Oxon.

Wang, J, Niu, D., and Zhang, Y., 2015. Mechanical properties, permeability and durability of accelerated shotcrete. Construction and Building Materials 95, 312–328.

FIGURE CAPTION

Fig. 1 Spraying the tunnel roof with the shotcrete spraying machine (picture courtesy Roland Mayr, BASF)

Fig. 2: Convergence-confinement method: Geometry of the problem and example of a convergence-confinement curve. Key: p: Internal tunnel pressure, R: Tunnel radius, r: Radial coordinate, u: Radial displacement of the tunnel wall, p_{cr}: Critical pressure (modified by Oreste, 2009).

Fig. 3 Convergence-confinement curve and reaction curve of the shotcrete lining with numerical integration of the reaction curve of the shotcrete lining and a calculation step. A is the interaction between reaction line and CCC to identify the final load process. Not to scale.

Fig. 4 Progressive increase of the asymptotic elastic modulus (A) and UCS (B) of the shotcrete with time for the two considered typologies in the example 1.

Fig. 5 Reaction curves of the SC lining as a function of the face advance rate (Va) and the mechanical characteristics of the shotcrete for the example 1.

Fig. 6 Variation of the rotation (A), normal displacement (B), shear displacement (C), bending moment (D), normal force (E) and shear force (F) for the two considered type of SC and two assumed advance rates (Va) of the tunnel face, with reference to the final equilibrium point (example 1).

Fig. 7 Reaction curve of the shotcrete lining (with enlargement on the right side) as a function of the face advance rate (Va) and the shotcrete type considered in the example 2.

Fig. 8 Variation of the rotation (A), normal displacement (B), shear displacement (C), bending moment (D), normal force (E) and shear force (F) for the two considered types of SC and two assumed velocities of advance (Va) of the tunnel face, with reference to the final equilibrium point (example 2).

Fig. 9 CCCs and reaction curve of the shotcrete lining (with enlargement on the right side) as a function of the velocity of advance (Va) and the final elastic modulus of the shotcrete, for example 3 (A) and example 4 (B).

Fig. 10 Variation of the rotation (A), normal displacement (B), shear displacement (C), bending moment (D), normal force (E) and shear force (F) for two considered types of SC and two assumed velocities of advance (Va) of the tunnel face, with reference to the final equilibrium point (example 3).

Fig. 11 Variation of the rotation (A), normal displacement (B), shear displacement (C), bending moment (D), normal force (E) and shear force (F) for the two considered types of SC and two assumed velocities of advance (Va) of the tunnel face, with reference to the final equilibrium point (example 4).

Fig. 12 CCCs of the tunnel and reaction lines of the shotcrete lining (with enlargement on the right side) as a function of the face velocity of advance (Va) and the shotcrete types for the example 5 (A) and 6 (B).

Fig. 13 Variation of the rotation (A), normal displacement (B), shear displacement (C), bending moment (D), normal force (E) and shear force (F) for the two considered types of SC and two assumed velocities of advance (Va) of the tunnel face, with reference to the final equilibrium point (example 5).

Fig. 14 Variation of the rotation (A), normal displacement (B), shear displacement (C), bending moment (D), normal force (E) and shear force (F) for the two considered types of SC and two assumed velocities of advance (Va) of the tunnel face, with reference to the final equilibrium point (example 6).